Journal of Materials Chemistry A

RSC Publishing

PAPER

View Article Online
View Journal | View Issue

Cite this: J. Mater. Chem. A, 2013, 1, 14766

Chemical exfoliation of graphitic carbon nitride for efficient heterogeneous photocatalysis†

Jing Xu,‡ Liwu Zhang,‡§ Rui Shi and Yongfa Zhu*

Received 13th August 2013
Accepted 26th September 2013

DOI: 10.1039/c3ta13188b

www.rsc.org/MaterialsA

Single atomic layer nanosheet materials show great application potential in many fields due to their enhanced intrinsic properties compared to their counterparts and newly born properties. Herein, g-C_3N_4 nanosheets with a single atomic layer structure are prepared by a simple chemical exfoliation method. The as-prepared nanosheets show a single atomic thickness of 0.4 nm and a lateral size of micrometers. The structure and photocatalytic properties of the as-prepared single layer g-C_3N_4 are then studied. Compared with the bulk g-C_3N_4, single layer g-C_3N_4 nanosheets show great superiority in photogenerated charge carrier transfer and separation. Accordingly, the photocatalytic H_2 production and pollutant decomposition activities and photocurrent generation of single layer g-C_3N_4 nanosheets are much higher than those of the bulk g-C_3N_4, indicating the great application potential of single layer g-C_3N_4 nanosheets in photocatalysis and photosynthesis.

1. Introduction

Single atomic layer nanosheets have attracted extensive attention due to their unique structural and physiochemical properties.[1] Since the discovery of the two-dimensional atomic crystal graphene,[2] which presents many intriguing properties different from bulk graphite and potential in diverse applications, great efforts have been made to synthesize nanosheets with single atomic layer structure.[3–7] By exfoliating layered materials into nanosheets, exotic electronic properties and high specific surface areas accompanied by greatly enhanced host capabilities have been obtained and show great potential in applications in electronics, energy storage, solar energy conversion, *etc.*[8,9]

Graphite-like carbon nitride (g-C_3N_4), a metal-free polymer semiconductor, has attracted plenty of attention due to its potential application in solar energy conversion, photosynthesis, electrocatalysis, bioimaging and biomedical application.[10–21] g-C_3N_4 has been shown to be able to produce H_2 by water splitting and decompose organic pollutants under visible light irradiation by the pioneering reports of Wang and coworkers.[22] More potential applications of g-C_3N_4 are emerging as studies being carried out on structure engineering and activity are improving.[12,23–31]

Motivated by graphene, researchers have tried to prepare the nanosheet form of g-C_3N_4 to fully explore the potential of g-C_3N_4. Compared with graphite, the layer of g-C_3N_4 is composed of C–N bonds instead of C–C bonds, and weak van der Waals force exists between the layers. Encouraged by the exfoliation of graphite into graphene layers by the widely used Hummers method,[32] Liu and coworkers employed the Hummers method to exfoliate bulk g-C_3N_4.[33] However, instead of nanosheets, particles with several hundred nanometer thickness were obtained and the planar atomic structure of g-C_3N_4 was destroyed, indicating that the Hummers method may destroy the intrinsic structure of g-C_3N_4. The failure is attributed to the not strong enough hydrogen bonding between the layers of strands of polymeric melon units with NH/NH_2 groups as proposed by Lotsch *et al.*,[34] which is different from the planar pure covalent bonding cohesion within the graphite. Liu and coworkers thus developed a direct thermal oxidation "etching" process of bulk g-C_3N_4 to get g-C_3N_4 nanosheets with a thickness of around 2 nm, implying a multilayer of g-C_3N_4 (6–7 layers).[33] Ultrathin g-C_3N_4 nanosheets were also prepared by ultrasound exfoliation or liquid exfoliation routes from bulk g-C_3N_4.[11,35] The resulted nanosheets possess thickness of >2 nm. Instead of the "top-down" fabrication of g-C_3N_4 nanosheets, Wang and coworkers found that a "bottom-up" method by modifying polycondensation of g-C_3N_4 precursors could result in thin C_3N_4 nanosheets with a thickness of around 3.6 nm.[36] Although different methods have successfully been developed to get g-C_3N_4 nanosheets, the as-prepared g-C_3N_4 nanosheets are still thicker than 2 nm and composed of more than 6 C–N layers. It is still a great challenge to prepare real graphene-like g-C_3N_4 materials with a single atomic layer.

Department of Chemistry, Tsinghua University, Beijing, 100084, PR China. E-mail: zhuyf@mail.tsinghua.edu.cn; zhanglw04@gmail.com

† Electronic supplementary information (ESI) available. See DOI: 10.1039/c3ta13188b

‡ These authors have contributed equally to this work.

§ Present address: Cavendish Laboratory, University of Cambridge, JJ Thomson Ave, Cambridge, CB3 0HE, UK.

Herein, we have for the first time obtained the single atomic layer g-C_3N_4 nanosheets (monolayer-C_3N_4) by a simple chemical exfoliation method. Since g-C_3N_4 is not strong enough against the strong oxidation effect exerted by the $KMnO_4$ oxidant used in the Hummers method for graphite exfoliation, $KMnO_4$ is no more used in the chemical exfoliation method. The obtained monolayer-C_3N_4 is then characterized and performances in photosynthesis and photocatalysis under visible light irradiation are investigated.

2. Experimental section

Synthesis of single atomic layer g-C_3N_4 nanosheets

g-C_3N_4 was prepared by heating dicyandiamide (Tianjin Fuchen Chemical Reagents factory, China) in a muffle furnace for 4 h to 550 °C and kept at this temperature for another 4 h in air. g-C_3N_4 monolayer nanosheets were synthesized *via* the chemical exfoliation method. The as-prepared g-C_3N_4 (1 g) was mixed with 10 mL of H_2SO_4 (98 wt %) in a 50 mL flask and stirred for 8 h at room temperature. Then the mixture was slowly poured into 100 mL of deionized water and sonicated for exfoliation. The temperature of the suspension increased rapidly, and the color changed from yellow to light yellow. The obtained suspension was then subjected to 10 min of centrifugation at 3000 rpm to remove any unexfoliated g-C_3N_4. The obtained light yellow suspension was centrifuged, washed thoroughly with deionized water to remove the residual acid, and finally dried at 80 °C in air overnight. In order to eliminate the structural defects, the obtained powders (0.3 g) were put into a flask with 150 mL of methanol and refluxed on a mantle heater at 65 °C for 6 h. After centrifugation and drying at 80 °C, the obtained products were g-C_3N_4 nanosheets.

Characterization of the samples

The samples were characterized by powder X-ray diffraction (XRD) on a Bruker D8-advance X-ray diffractometer at 40 kV and 40 mA for monochromatized Cu Kα ($\lambda = 1.5406$ Å) radiation. The Brunauer–Emmett–Teller (BET) specific surface area and pore volume of the samples were characterized by nitrogen adsorption at 77 K with Micromeritics 3020 instrument. Transmission electron microscopy (TEM) images were obtained by Hitachi HT-7700 electron microscope operated at an accelerating voltage of 100 kV. Atomic Force Microscope (AFM) images were acquired in phase mode in air using a Digital Instrument Shimadzu SPM-9600 (The samples were prepared by drop-casting corresponding dilute dispersions onto freshly cleaved mica surface). Fourier transformed infrared (FTIR) spectra were recorded on a Bruker VERTEX 700 spectrometer between 4000 and 600 cm^{-1}. Diffuse reflection spectra (DRS) were obtained on a Hitachi U-3010 UV-vis spectrophotometer. Photoluminescence spectra (PL) of the samples were obtained at room temperature excited by incident light of 318 nm using a fluorescence spectrometer (JASCO FP-6500). Elemental analysis results were collected from an EA 3000 analyzer.

Photocatalytic tests and photoelectrochemical performance

The photocatalytic activities for H_2 production were evaluated under visible light irradiation ($\lambda > 420$ nm). Visible irradiation was provided by a 500 W xenon lamp with a 420 nm cutoff filter and the average visible light intensity was 40.0 mW cm^{-2}. 20 mg of the photocatalyst powder was dispersed in an aqueous solution (20 mL) containing triethanolamine (10 vol%) as a sacrificial electron donor. 3 wt% Pt was loaded on the surface of the photocatalyst sample by the *in situ* photodeposition method using H_2PtCl_6. The suspension solution was then purged with N_2 for at least 30 min to remove air and then sealed with a rubber septum. The temperature of the reaction solution was maintained at room temperature by a flow of cooling water during the photocatalytic reaction. The amount of evolved hydrogen was analyzed using a Shimadzu GC-2014 gas chromatograph equipped with a thermal conductive (TCD) detector and a 5 Å molecular sieve column, using N_2 as the carrier gas.

The photocatalytic activities were further evaluated by the degradation of phenol and methylene blue (MB) under visible light irradiation. In each run, 50 mL of MB solution (2.0×10^{-5} M) or phenol solution (2.0 mg L^{-1}) containing 25 mg of as-synthesized photocatalyst were placed in a glass beaker. Before irradiation, the suspensions were magnetically stirred in the dark for 2 h to ensure equilibrium between the photocatalyst and the model molecules. At certain time intervals, 2 mL of the suspensions were taken and centrifuged to remove the particles. The concentration of phenol was analyzed using a HPLC with a UV absorbance detector operated at 270 nm coupled to a Venusil XBP-C18 column. The concentration of the MB was analyzed by recording the absorption intensity at 663 nm using a Hitachi U-3010 UV-vis spectrophotometer.

The photoelectrochemical properties were investigated on a CHI 660B electrochemical system (Shanghai, China) using a standard three-electrode cell with a working electrode, a platinum wire counter electrode, and a standard calomel electrode (SCE) reference electrode. 0.1 M Na_2SO_4 was used the electrolyte. The working electrodes were prepared as follows: 2 mg of the as-prepared photocatalyst was suspended in 1 mL of water to produce a slurry, which was then dip-coated on a 20 mm × 40 mm indium-tin oxide (ITO) glass electrode. The electrodes were exposed in air for 1 day to eliminate water and subsequently heated at 200 °C for 1 day. All investigated working electrodes were of similar thickness. Electrochemical impedance spectroscopy (EIS) was carried out at the open circuit potential. A sinusoidal ac perturbation of 5 mV was applied to the electrode over the frequency range 0.05 to 10^5 Hz.

3. Results and discussion

The synthetic strategy is illustrated in Fig. 1. First, the bulk g-C_3N_4 was mixed with H_2SO_4 (98 wt%) and stirred for 8 hours at room temperature to allow the intercalation of H_2SO_4 in the interlayer space of g-C_3N_4. The intercalation mechanism is generally similar to the widely reported H_2SO_4 intercalated graphite.[37] The intercalation of H_2SO_4 into bulk g-C_3N_4 is confirmed by X-ray diffraction (XRD) (Fig. 2). It is found that the

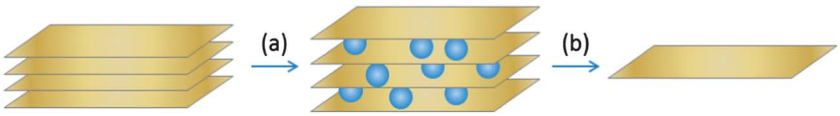

Fig. 1 Illustration of synthetic strategy. (a) Intercalation of H_2SO_4 (98 wt%) in the interplanar space of g-C_3N_4. (b) Intercalated g-C_3N_4 was exfoliated into a single layer due to the rapid heating effect of H_2SO_4 (98 wt%) mixing with water.

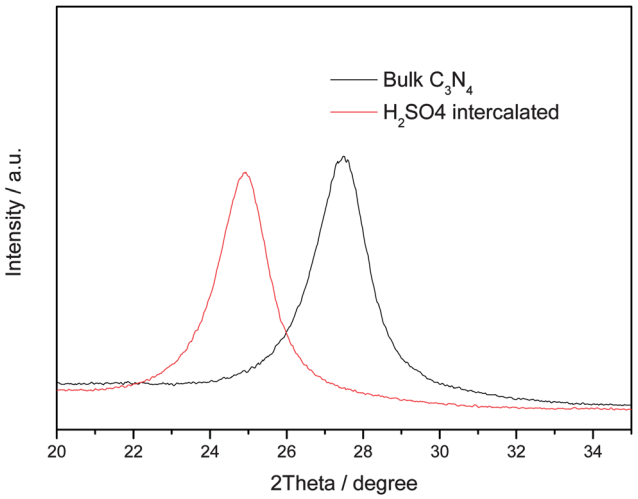

Fig. 2 XRD patterns of the bulk g-C_3N_4 before and after H_2SO_4 intercalation.

(002) diffraction at around 27.4° relating to the characteristic interlayer stacking structure is shifted to 25.0°, indicating that the interlayer distance is expanded from 0.325 nm to 0.356 nm. Then the mixture was slowly poured into deionized water and sonicated, due to the sonication and rapid heating effect when concentrated H_2SO_4 is mixed with water, the intercalated bulk g-C_3N_4 was exfoliated into a single layer. The obtained dispersion was then subjected to centrifugation to remove any unexfoliated and aggregated g-C_3N_4. The exfoliation is found to significantly depend on the concentration of sulfuric acid. H_2SO_4 with lower concentrations (75 wt% and 50 wt%) were also studied, however the results show that lower concentration H_2SO_4 failed to exfoliate bulk g-C_3N_4 into a single layer (Fig. S1 and S2 in the ESI†). Compared with the reported thermal oxidation "etching" process,[33] the ultrasound exfoliation[11] or "bottom-up" method[36] for the fabrication of g-C_3N_4 nanosheets, the chemical exfoliation method allows intercalation of H_2SO_4 in the interlayer space of g-C_3N_4, thus higher possibility to obtain a single layer nanosheet after exfoliation. Moreover, the chemical exfoliation method is also more cost-efficient than the reported methods mentioned above.

Fig. 3a shows the typical atomic force microscopic (AFM) image of the exfoliated g-C_3N_4 nanosheets. The lateral size of these sheets ranges from tens of nanometers to several micrometers. The thickness analysis of the nanosheets by AFM reveals an average thickness of about 0.4 nm, which is very close to the theoretical thickness of monolayer g-C_3N_4 (about 0.325 nm). Statistical studies of the thickness of single layer g-C_3N_4 nanosheets by measuring different samples confirm this observation (Fig. S3 in the ESI†). Some multilayered g-C_3N_4 nanosheets with thickness from 1 nm to 4 nm are also observed in the AFM studies, which comprise *ca.* 40% of the sample, indicating that the current chemical exfoliation can produce g-C_3N_4 nanosheets with 60% single layer C_3N_4. The TEM image (Fig. 3b) illustrates the very transparent feature of the nanosheets, indicating the ultrathin thickness of the nanosheets. The darker part in the TEM image can be attributed to the overlap of several g-C_3N_4 nanosheets or a multilayer nanosheet. The bulk g-C_3N_4 before exfoliation shows a thickness of more than 10 nm (Fig. S4 and S5†), indicating the effectiveness of the current chemical exfoliation method. The EDX studies (Fig. S6†) confirmed the elemental composition of the nanosheets, which are shown to be composed of C and N elements, while the Cu detected can be attributed to the copper substrate for TEM investigation. Notably, oxygen is not detected in the elemental analysis of the nanosheets, implying that the g-C_3N_4 is not oxidized by concentrated H_2SO_4 employed for exfoliation.

The structure, composition and chemical states of the monolayer-C_3N_4 is further investigated by XRD, X-ray photoelectron spectroscopy (XPS), Fourier transform infrared spectroscopy (FTIR), *etc.* In the XRD patterns (Fig. 4a), the (002) diffraction at around 27.4° relates to the characteristic interlayer stacking structure, while the (100) diffraction at 13.0° indicates the interplanar structural packing. It has been reported in some other monolayer structures that due to the formation of agglomerates and crumples of the monolayer nanosheets by van der Waals force during preparation of the sample for XRD measurement, the XRD pattern of the monolayer nanosheets could resemble that of the bulk form.[38–40] However, it is observed that the intensity of (002) diffraction related to the interlayer stacking is significantly weakened after exfoliation as expected. The multilayer components in the sample also contribute to the observed (002) diffraction.

The strong FTIR absorption bands of monolayer-C_3N_4 in Fig. 4b and c further revealed a typical molecular structure of graphitic carbon nitride. The absorption bands near 1572 and 1632 cm^{-1} are attributed to C=N stretching, while the three bands at 1253, 1320 and 1425 cm^{-1} correspond to aromatic C–N stretching. The peak at 807 cm^{-1} belongs to triazine ring mode, which corresponds to condensed CN heterocycles. The broad band at 3000–3500 cm^{-1} corresponds to uncondensed terminal amino groups (–NH_2 or =NH groups). The FTIR results are in fairly good accordance with the reports of g-C_3N_4 materials prepared by polycondensation and polymerization reactions.[25,26] The Raman spectra are also investigated to confirm the molecular structure of g-C_3N_4 (Fig. S7 in the ESI†). In the Raman spectra for both bulk and monolayer g-C_3N_4, there are two characteristic bands related to the disordered D (around 1300 cm^{-1}) and graphitic G (around 1500 cm^{-1}) bands,

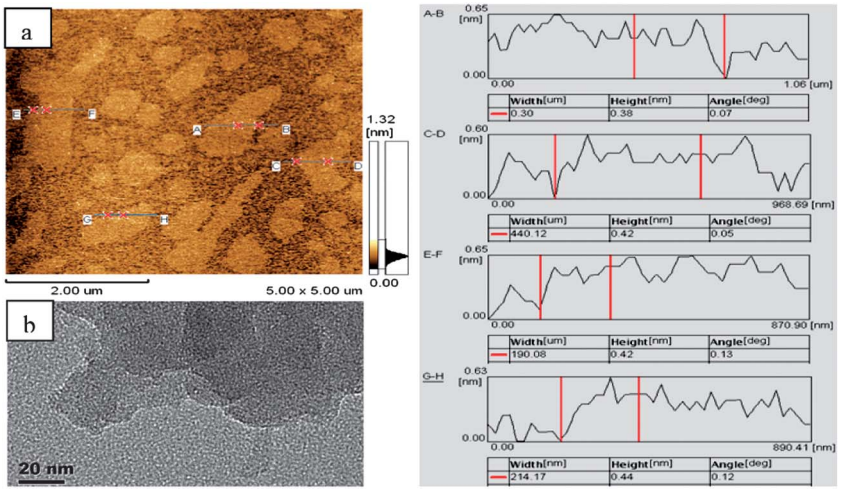

Fig. 3 Typical AFM images (a) and TEM images (b) of the as-prepared monolayer-C_3N_4 nanosheets. The tables and curves in the right panel show the height and width information of different nanosheets from the AFM images.

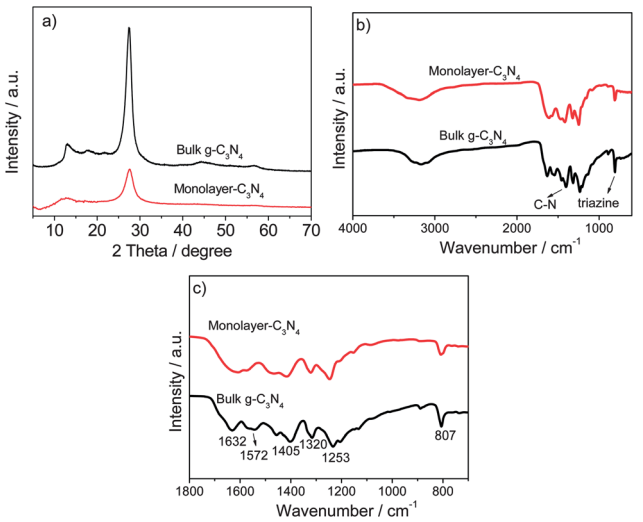

Fig. 4 (a) XRD patterns, (b) FTIR spectra, and (c) enlarged FTIR spectra of the bulk g-C_3N_4 and monolayer-C_3N_4.

indicating the formation of the graphitic structure. The Raman bands at 600–800 cm^{-1} can be attributed to the in-plane rotation of sixfold rings in a graphitic carbon nitride layer.[41]

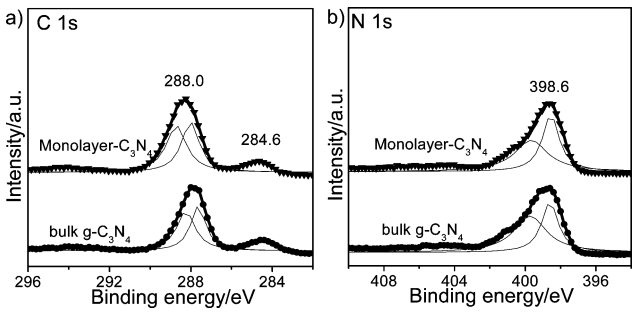

Fig. 5 (a) C1s XPS spectra; (b) N1s XPS spectra of the bulk g-C_3N_4 and monolayer-C_3N_4 nanosheets.

The chemical states of the monolayer-C_3N_4 and the bulk g-C_3N_4 were studied by XPS (Fig. 5). The C1s spectra show two peaks located at about 284.6 eV and 288.0 eV. The 288.0 eV peak is further deconvoluted into two Gaussian–Lorenzian peaks. The main contribution peak at 287.9 eV is attributed to the sp^2 hybridized carbon bonded to N inside the triazine rings, while the peak at 288.6 is assigned to the sp^2 hybridized carbon in the triazine ring bonded to the $-NH_2$ group.[35] The peak at 284.6 eV is typically ascribed to sp^2 C=C bonds. The peak of 398.6 eV in the N1s spectra can also be deconvoluted into two Gaussian–Lorenzian peaks. The dominant peak at 398.7 eV corresponds to the sp^2-bonded N involved in the triazine rings (C–N=C), while the peak at 399.7 eV is attributed to the bridging N atoms in N–$(C)_3$ or N bonded with hydrogen.[35]

The optical properties have been investigated by UV-Vis diffuse reflectance spectra (DRS) and photoluminescence (PL) measurements (Fig. 6a and b). It is found that the absorption edge of monolayer-C_3N_4 shows a remarkable blue shift from 470 to 425 nm, corresponding to an increase in the band gap from 2.64 eV to 2.92 eV compared with that of bulk g-C_3N_4. This blue shift performance can be presumably ascribed to the decrease of conjugation length and the strong quantum confinement effect due to the single layer structure of g-C_3N_4 nanosheets. The PL spectra demonstrate that under photoexcitation at 318 nm, the emission peak of the bulk g-C_3N_4 locates at around 464 nm, while the position of the emission peak is blue shifted to 438

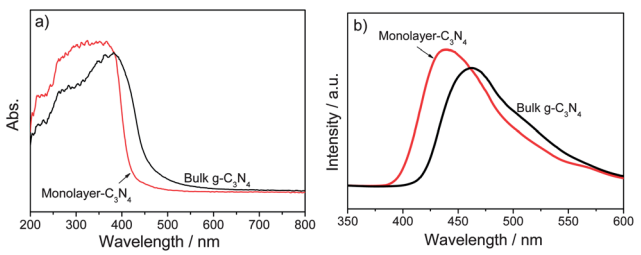

Fig. 6 (a) DRS spectra and (b) PL spectra of the bulk g-C_3N_4 and monolayer-C_3N_4.

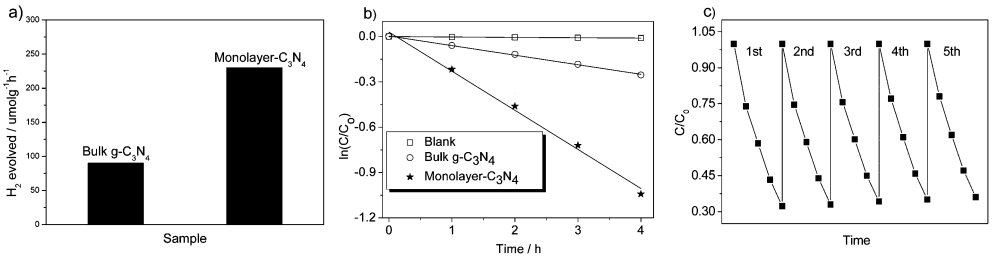

Fig. 7 (a) Photocatalytic H_2 production on bulk-C_3N_4 and monolayer-C_3N_4. (b) Photocatalytic decomposition of phenol under visible light irradiation (λ >420 nm). (c) Stability measurement.

nm in the case of monolayer-C_3N_4. The blue shift of the emission peak by 26 nm is in good agreement with the larger bandgap by 0.28 eV of monolayer-C_3N_4 nanosheets.

The photocatalytic H_2 production from water in the presence of the bulk g-C_3N_4 or monolayer-C_3N_4 were studied under visible-light irradiation ($\lambda > 420$ nm), as shown in Fig. 7a. 3 wt% Pt was loaded on the surface of the photocatalyst samples by the *in situ* photodeposition method from H_2PtCl_6 solution. It is found that monolayer-C_3N_4 shows a significant improvement over the reference bulk g-C_3N_4. The rate of H_2 evolution on monolayer-C_3N_4 reaches 230 μmol g^{-1} h^{-1}, which is about 2.6 times the rate of the bulk g-C_3N_4 (90 μmol g^{-1} h^{-1}).

The superiority of monolayer-C_3N_4 for photocatalysis application is further confirmed by the photodegradation of phenol under visible light irradiation. A first-order linear relationship was revealed by the plots of $\ln(C/C_0)$ *versus* irradiation time (Fig. 7b). The determined reaction-rate constants, k, were 0.0633 and 0.2589 h^{-1}, respectively, for bulk g-C_3N_4 and monolayer-C_3N_4. The photocatalytic decomposition rate over the monolayer nanosheet was more than four times as fast as the bulk g-C_3N_4. The monolayer-C_3N_4 also shows a more than threefold enhancement in the photocatalytic degradation of methylene blue under visible light irradiation, as shown in Fig. S8 in the ESI.† The stability of the monolayer-C_3N_4 as a photocatalyst is also evaluated under visible light irradiation (Fig. 7c). It is found that the photocatalytic activity only very slightly decreased after five successive cycles of photocatalysis degradation tests, indicating the monolayer-C_3N_4 is fairly stable under the studied conditions.

It is well known that the photocatalytic activity is greatly related to the surface area, charge transport, light absorption and so on. The properties and photocatalytic activity of the single atomic layer g-C_3N_4 are different from multilayer g-C_3N_4 mainly in three aspects: (i) the electron and hole mobilities in the monolayer are significantly greater than those in the multilayer, which has been proved in the study of graphene. (ii) The surface area of the monolayer is bigger than that of the multilayer, which is also very important for a photocatalyst. (iii) The light absorption is different due to the quantum size effect, the absorption edge is expected to be more blue-shifted in the case of the monolayer, which could affect the photocatalytic activity by shifting the position of conduction and valence bands of g-C_3N_4. Since the monolayer-C_3N_4 was obtained from bulk g-C_3N_4 by chemical exfoliation, the crystallinity should be similar in both materials, which is also confirmed by the XRD patterns. Therefore, the greatly enhanced photocatalytic activity of monolayer-C_3N_4 than the bulk g-C_3N_4 in both H_2 production and phenol degradation can be attributed to several reasons: first, the increased surface area, the measured surface area of monolayer-C_3N_4, is 205.8 m^2 g^{-1}, which is almost 50 times larger than that of bulk-C_3N_4 (4.3 m^2 g^{-1}), suggesting more active sites in the monolayer-C_3N_4 for photocatalytic reaction. Secondly, the improved photogenerated charge carrier transportation and separation due to the monolayer nanosheet structure. The monolayer nanosheet structure can significantly reduce the distance for the charge carriers to transfer from the place generated to the solid–liquid interface due to the ultrathin structure. Finally, the negatively shifted conduction band due to the quantum size effect can increase the activity of photogenerated electrons.

The improved charge carrier separation in monolayer-C_3N_4 is investigated by the photocurrent and electrochemical impedance spectroscopy (EIS) measurements (Fig. 8). The potential of the electrodes against a Pt counter electrode was set at 0.0 V *vs.* saturated calomel electrode (SCE). As shown in Fig. 8a, a fast and uniform photocurrent response was observed for each switch-on and switch-off event in both bulk g-C_3N_4 and monolayer-C_3N_4 electrodes. This photoresponsive phenomenon was entirely reversible. The photocurrent of the monolayer-C_3N_4 is about four times as high as that of the bulk g-C_3N_4 electrode, which indicates that the separation efficiency of photoinduced electrons and holes is significantly improved in the monolayer-C_3N_4 nanosheet.

The effect of the monolayer nanosheet structure on the kinetics of interfacial charge transfer was confirmed by EIS. Fig. 8b shows the EIS Nyquist plots of the bulk g-C_3N_4 and monolayer-C_3N_4 electrodes in the dark or under visible light

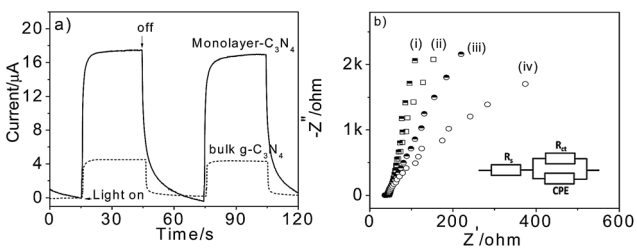

Fig. 8 (a) Photocurrent response under chopped illumination. (b) The EIS response of bulk g-C_3N_4 ((i) dark, (ii) under visible light irradiation) and monolayer-C_3N_4 electrodes ((iii) dark, (iv) under visible light irradiation).

irradiation. The Nyquist plot was also fitted to the equivalent Randle circuit (Fig. 8b, inset), where R_s is the electrolyte solution resistance, CPE is the constant phase element for the electrode and electrolyte interface, and R_{ct} is the interfacial charge transfer resistance across the electrode/electrolyte. A lower value of R_{ct} suggests more efficient charge transfer across the electrode/electrolyte interface, reducing the possibility of charge recombination and thus enhancing the photocurrent response.[42] The fitted R_{ct} values for the bulk g-C_3N_4 and monolayer-C_3N_4 under visible light irradiation are 2570.7 and 980.2 Ω, respectively, indicating that the monolayer-C_3N_4 possesses more efficient charge transfer than the bulk g-C_3N_4. One possible reason for the more efficient charge transport in nanosheets than the bulk g-C_3N_4 could be the electron–phonon interaction in the material. The lattice photons are different in the low dimension material, which could affect the conductivity of the material. The efficient charge mobility has been observed in low dimension materials, one typical example is graphene, which shows very high electron mobility.[2] However, the exact mechanism is still not very clear.

4. Conclusion

In summary, we have successfully obtained single atomic layer g-C_3N_4 nanosheets by a simple chemical exfoliation of the bulk g-C_3N_4. Although there is still 40% of multilayer nanosheets existing in the product, it is the first time that single layer g-C_3N_4 nanosheets are produced. Compared with the bulk g-C_3N_4, single layer g-C_3N_4 nanosheets show much larger surface area and great superiority in photogenerated charge carrier transport. Accordingly, the photocatalytic activity and photocurrent of single layer g-C_3N_4 nanosheets are significantly enhanced. A threefold enhancement in photocatalytic H_2 production is observed in the single layer nanosheet as a photocatalyst. Experiments trying to separate the single layer nanosheets from the multilayer ones are underway. The single layer g-C_3N_4 shows great potential in application both in environment purification and solar energy conversion.

Acknowledgements

The project was supported by the National Basic Research Program of China (973) (2013CB632403), National High Technology Research and Development Program of China (863) (2012AA062701), Chinese National Science Foundation (20925725 and 21373121), and Atmospheric Environment Monitoring & Pollution Control Program of Jiangsu Province (AEMPC201103).

References

1 A. K. Geim and K. S. Novoselov, *Nat. Mater.*, 2007, **6**, 183.
2 K. S. Novoselov, A. K. Geim, S. V. Morozov, D. Jiang, Y. Zhang, S. V. Dubonos, I. V. Grigorieva and A. A. Firsov, *Science*, 2004, **306**, 666.
3 Z. Y. Zeng, Z. Y. Yin, X. Huang, H. Li, Q. Y. He, G. Lu, F. Boey and H. Zhang, *Angew. Chem., Int. Ed.*, 2011, **50**, 11093.
4 T. Brugger, H. F. Ma, M. Iannuzzi, S. Berner, A. Winkler, J. Hutter, J. Osterwalder and T. Greber, *Angew. Chem., Int. Ed.*, 2010, **49**, 6120.
5 G. Eda, T. Fujita, H. Yamaguchi, D. Voiry, M. W. Chen and M. Chhowalla, *ACS Nano*, 2012, **6**, 7311.
6 S. Helveg, J. V. Lauritsen, E. Laegsgaard, I. Stensgaard, J. K. Norskov, B. S. Clausen, H. Topsoe and F. Besenbacher, *Phys. Rev. Lett.*, 2000, **84**, 951.
7 J. Feng, L. Peng, C. Wu, X. Sun, S. Hu, C. Lin, J. Dai, J. Yang and Y. Xie, *Adv. Mater.*, 2012, **24**, 1917.
8 J. N. Coleman, M. Lotya, A. ONeill, S. D. Bergin, P. J. King, U. Khan, K. Young, A. Gaucher, S. De, R. J. Smith, I. V. Shvets, S. K. Arora, G. Stanton, H.-Y. Kim, K. Lee, G. T. Kim, G. S. Duesberg, T. Hallam, J. J. Boland, J. J. Wang, J. F. Donegan, J. C. Grunlan, G. Moriarty, A. Shmeliov, R. J. Nicholls, J. M. Perkins, E. M. Grieveson, K. Theuwissen, D. W. McComb, P. D. Nellist and V. Nicolosi, *Science*, 2011, **331**, 568.
9 J.-w. Seo, Y.-w. Jun, S.-w. Park, H. Nah, T. Moon, B. Park, J.-G. Kim, Y. J. Kim and J. Cheon, *Angew. Chem.*, 2007, **119**, 8984.
10 G. Liu, P. Niu, C. H. Sun, S. C. Smith, Z. G. Chen, G. Q. Lu and H. M. Cheng, *J. Am. Chem. Soc.*, 2010, **132**, 11642.
11 X. Zhang, X. Xie, H. Wang, J. Zhang, B. Pan and Y. Xie, *J. Am. Chem. Soc.*, 2013, **135**, 18.
12 Y. Zhang, A. Thomas, M. Antonietti and X. Wang, *J. Am. Chem. Soc.*, 2009, **131**, 50.
13 Z. H. Zhang, K. Leinenweber, M. Bauer, L. A. J. Garvie, P. F. McMillan and G. H. Wolf, *J. Am. Chem. Soc.*, 2001, **123**, 7788.
14 J. Sun, J. Zhang, M. Zhang, M. Antonietti, X. Fu and X. Wang, *Nat. Commun.*, 2012, **3**, 1139.
15 F. Goettmann, A. Thomas and M. Antonietti, *Angew. Chem., Int. Ed.*, 2007, **46**, 2717.
16 X. Jin, V. V. Balasubramanian, S. T. Selvan, D. P. Sawant, M. A. Chari, G. Q. Lu and A. Vinu, *Angew. Chem., Int. Ed.*, 2009, **48**, 7884.
17 E. Z. Lee, Y. S. Jun, W. H. Hong, A. Thomas and M. M. Jin, *Angew. Chem., Int. Ed.*, 2010, **49**, 9706.
18 Y. Wang, J. S. Zhang, X. C. Wang, M. Antonietti and H. R. Li, *Angew. Chem., Int. Ed.*, 2010, **49**, 3356.
19 J. S. Zhang, G. G. Zhang, X. F. Chen, S. Lin, L. Mohlmann, G. Dolega, G. Lipner, M. Antonietti, S. Blechert and X. C. Wang, *Angew. Chem., Int. Ed.*, 2012, **51**, 3183.
20 W. Schnick, *Angew. Chem., Int. Ed.*, 1993, **32**, 1580.
21 Q. Xiang, J. Yu and M. Jaroniec, *J. Phys. Chem. C*, 2011, **115**, 7355.
22 X. C. Wang, K. Maeda, A. Thomas, K. Takanabe, G. Xin, J. M. Carlsson, K. Domen and M. Antonietti, *Nat. Mater.*, 2009, **8**, 76.
23 Y. J. Cui, Z. X. Ding, X. Z. Fu and X. C. Wang, *Angew. Chem., Int. Ed.*, 2012, **51**, 11814.
24 J. Liang, Y. Zheng, J. Chen, J. Liu, D. Hulicova-Jurcakova, M. Jaroniec and S. Z. Qiao, *Angew. Chem., Int. Ed.*, 2012, **51**, 3892.
25 F. Z. Su, S. C. Mathew, L. Mohlmann, M. Antonietti, X. C. Wang and S. Blechert, *Angew. Chem., Int. Ed.*, 2011, **50**, 657.

26 Y. Wang, X. C. Wang and M. Antonietti, *Angew. Chem., Int. Ed.*, 2012, **51**, 68.
27 J. S. Zhang, M. W. Zhang, R. Q. Sun and X. C. Wang, *Angew. Chem., Int. Ed.*, 2012, **51**, 10145.
28 X. F. Chen, J. S. Zhang, X. Z. Fu, M. Antonietti and X. C. Wang, *J. Am. Chem. Soc.*, 2009, **131**, 11658.
29 F. Z. Su, S. C. Mathew, G. Lipner, X. Z. Fu, M. Antonietti, S. Blechert and X. C. Wang, *J. Am. Chem. Soc.*, 2010, **132**, 16299.
30 Y. Zheng, Y. Jiao, J. Chen, J. Liu, J. Liang, A. Du, W. M. Zhang, Z. H. Zhu, S. C. Smith, M. Jaroniec, G. Q. Lu and S. Z. Qiao, *J. Am. Chem. Soc.*, 2011, **133**, 20116.
31 J. Yu, S. Wang, B. Cheng, Z. Lin and F. Huang, *Catal. Sci. Technol.*, 2013, **3**, 1782.
32 W. S. Hummers and R. E. Offeman, *J. Am. Chem. Soc.*, 1958, **80**, 1339.
33 P. Niu, L. Zhang, G. Liu and H.-M. Cheng, *Adv. Funct. Mater.*, 2012, **22**, 4763.
34 B. V. Lotsch, M. Doblinger, J. Sehnert, L. Seyfarth, J. Senker, O. Oeckler and W. Schnick, *Chem.–Eur. J.*, 2007, **13**, 4969.
35 S. Yang, Y. Gong, J. Zhang, L. Zhan, L. Ma, Z. Fang, R. Vajtai, X. Wang and P. M. Ajayan, *Adv. Mater.*, 2013, **25**, 2452.
36 Z. Lin and X. Wang, *Angew. Chem., Int. Ed.*, 2013, **52**, 1735.
37 A. Moissette, H. Fuzellier, A. Burneau, J. Dubessy, D. Guerard and M. Lelaurain, in *Mater. Sci. Forum, Trans Tech Publ*, 1992, p. 95.
38 L. Li, Z. Chen, Y. Hu, X. Wang, T. Zhang, W. Chen and Q. Wang, *J. Am. Chem. Soc.*, 2013, **135**, 1213.
39 Y. Min, G. D. Moon, B. S. Kim, B. Lim, J.-S. Kim, C. Y. Kang and U. Jeong, *J. Am. Chem. Soc.*, 2012, **134**, 2872.
40 D. Li, M. B. Muller, S. Gilje, R. B. Kaner and G. G. Wallace, *Nat. Nanotechnol.*, 2008, **3**, 101.
41 A. Andreyev, M. Akaishi and D. Golberg, *Diamond Relat. Mater.*, 2002, **11**, 1885.
42 S. J. Hong, S. Lee, J. S. Jang and J. S. Lee, *Energy Environ. Sci.*, 2011, **4**, 1781.

